Corrosion Resistance Conferred by Superhydrophobic Fluorinated Polyacrylate–Silica Composite Coatings on Cold-Rolled Steel

Chang-Jian Weng, Chih-Wei Peng, Chi-Hao Chang, Ya-Han Chang, Jui-Ming Yeh

Department of Chemistry and Center for Nanotechnology, Chung Yuan Christian University, Chung Li, Taiwan 32023, Republic of China

Received 27 April 2011; accepted 18 October 2011
DOI 10.1002/app.36380
Published online in Wiley Online Library (wileyonlinelibrary.com).

ABSTRACT: The superhydrophobic surface (SHS) applied for corrosion protection in this study was prepared from an organic fluorinated polyacrylate incorporated with methyltriethoxysilane (MTES)-based silsesquioxanes spheres. The SHS, with a contact angle of about 153.2°, was coated onto the surface of cold-rolled steel (CRS) with spin-coating technology. The coating materials applied as anticorrosive coatings were based on a series of electrochemical corrosion-protection measurements in saline conditions. The SHS coating on CRS was found to provide superior corrosion protection to that of the hydrophobic organic coating in a series of electrochemical measurements in 3.5 wt % aqueous NaCl electrolyte. This form of coating could also provide better corrosion protection to coated CRS substrates and could serve as an effective barrier against aggressive species. © 2012 Wiley Periodicals, Inc. J Appl Polym Sci 000: 000–000, 2012

Key words: coatings; fluoropolymers; surface modification

INTRODUCTION

Metal corrosion consumes a significant part of the gross domestic product (GDP) of an industrialized country.[1] In the case of iron, chromate-based organic coatings offer effective corrosion protection, but environmental concerns have increasingly restricted their use.[2] Although anodization[3] is found to increase the thickness of the oxide layer, it nevertheless retains its porous nature.[4] Recently, layered materials, such as anionic clays (e.g., layered double hydroxide[5,6]) and cationic clays (e.g., montmorillonite[7]), have found use as additives in organic anticorrosion coatings or as polymer–clay nanocomposite corrosion-resistant coatings. Zeolites[8,9] have also been explored as corrosion-resistant coating materials. Hydrophobic self-assembled monolayers[10] of surfactant molecules that adhere to the surface have also been proposed recently as corrosion inhibitors, but they suffer from drawbacks, such as a limited stability of layers and miniscule-sized defects, which can allow aggressive species to reach the substrate surface.

Recent discoveries have connected the high water repellency of the lotus plant to its distinctive morphological properties, which form the basis for superhydrophobic surfaces (SHSs; i.e., surface contact angle with water $> 150°$). This finding has attracted the interest of many researchers and has pushed them to develop a biomimetic approach to generation a similar effect. The prospect of producing SHSs suggests huge opportunities in the following areas: (1) corrosion inhibition for metal components, (2) chemical and biological agent protection for clothing, and (3) antifouling for marine vehicles, among other applications. Researchers have since been successful in reproducing this superhydrophobic character using various methods; these have resulted in different means of surface modification.

Recently, a new way of strengthening corrosion resistance through the application of an anodic layer to the surface of metals has been described in the literature. Monocarboxylic acids [CH_3—$(CH_2)_n$—COOH] are environmentally friendly and have been known to act as corrosion inhibitors for various metals, including copper,[11] lead,[12] mild steel,[13,14] aluminum alloys,[15] and magnesium alloys.[16] This approach is characterized by the adsorption of the carboxylate group (negatively charged) on the metal surface (positively charged);[17,18] this allows the formation of a hydrophobic or a superhydrophobic film,[19–23] which then provides the corrosion protection. This demonstrates that monocarboxylic acid protects the alloys by reacting with the outer layer of the anodic film. This protective film renders the surface water resistant and significantly enhances its corrosion resistance.

Correspondence to: J.-M. Yeh (juiming@cycu.edu.tw).

Contract grant sponsor: Ministry of Education, Taiwan, Republic of China; contract grant number: NSC 98-2113-M-033-001-MY3.

Contract grant sponsor: Department of Chemistry at Chung Yuan Christian University; contract grant number: CYCU-98-CR-CH.

However, to date, the corrosion protection conferred by SHSs via polymer coating materials has rarely been reported. In this article, we discuss an SHS developed with organic fluorinated polyacrylate (FPA) and MTES-based silsesquioxanes spheres successfully prepared and applied as an anticorrosive coating. The effectiveness of the SHS was evaluated on the basis of a series of electrochemical corrosion protection measurements under saline conditions. The static contact angle of the applied SHS was found to be 153 ± 2°. The SHS coating on the cold-rolled steel (CRS) electrode was also found to be superior in terms of corrosion protection to a plain organic coating without the incorporation of MTES-based silsesquioxane spheres on the basis of a series of electrochemical measurements for corrosion potential (E_{corr}), polarization resistance, and corrosion current (I_{corr}) in 3.5 wt % aqueous NaCl electrolyte.

EXPERIMENTAL

Materials and instrumentations

Tetraethyl orthosilicate (Fluka, United States), methyl triethoxysilane (Fluka), ammonium hydroxide (Riedel-Dehaën, United States), benzoyl peroxide (BPO; Riedel-Dehaën, United States), methyl ethyl ketone (MEK; Riedel-Dehaën, United States), and ethanol (Riedel-Dehaën, United States) were used as received without further purification. Methyl methacrylate (Riedel-Dehaën, United States) and perfluorooctylethyl acrylate (Kyoeisha, Japan) were doubly distilled before use.

Attenuated total reflectance (ATR) Fourier transform infrared (FTIR) spectra were obtained at a resolution of 4.0 cm^{-1} with an FTIR instrument (JASCO, FT/IR-4100, Japan) at room temperature with a range of 4000–700 cm^{-1}. Surface-modified silica spheres were studied with ^{13}C and ^{29}Si solid-state magic angle spinning (MAS) NMR spectra. MAS NMR spectra were recorded at 9.4 T with a Bruker Avance 400 spectrometer with zirconia rotors 4 mm in diameter spun at 5 kHz. The ^{13}C spectra were obtained with a Bruker MSL500 instrument at 125 MHz with the cross-polarization (CP) technique and with tetramethylsilane (TMS) as a reference. The surface morphology of the films was observed with scanning electron microscopy (SEM; Hitachi S-4200, Japan) and atomic force microscopy (AFM; PSIA XE-100, United States). The particle size distribution was determined with a dynamic light scattering particle size analyzer (Brookhaven 90 plus, United States). The contact angle of the sample was measured with a First Ten Angstroms FTA 125. Electrochemical measurement was performed with VoltaLab 50 (France) instrument. A three-electrode configuration was employed in the circuit with the sample as the working electrode, a carbon counter electrode, and a saturated calomel electrode (SCE) as the reference electrode. The area of the working electrode was 1 cm^2. All of the measured potentials presented in this article refer to this electrode. All tests were performed at 30 ± 0.5°C in a corrosive medium (3.5 wt % aqueous NaCl). Before polarization current (Tafel extrapolation) measurement, 1 h of immersion in the medium was done to ensure steady-state conditions. For the polarization current experiments, the potential was scanned from −500 to +500 mV at a scan rate of 1 mV/s. I_{corr} was determined by superimposition of a straight line along the linear portion of the cathodic or anodic curve and its extrapolation through E_{corr}.

Synthesis of the hydrophobic surface (HS) coating material

The preparation of the HS coating material was done as follows: 30 mmol of MMA, 13 mmol of perfluorooctylethyl acrylate, 0.4 mmol of BPO, and 40 g of MEK were introduced into a 250-mL, three-necked, round-bottom flask. Under magnetic stirring, the solution was heated to 75°C for 24 h and then let cool to room temperature. The bulk solution was denoted as the FPA solution [Fig. 1(a)]. The FPA solution was coated onto one side of the CRS substrate at 1500 rpm and then dried under ambient conditions at 110°C for 15 min in an oven [Fig. 1(c)].

Synthesis of the MTES-based silsesquioxane spheres

The preparation of the MTES-based silsesquioxane spheres was performed as follows: 3 mL of 28% ammonium hydroxide was dissolved in 30 mL of ethanol and then transferred into a 100-mL, two-necked, round-bottom flask. The entire mixture was heated to 75°C for 30 min under stirring. Subsequently, 28 mmol of methyl triethoxysilane and 24 mmol of tetraethyl orthosilicate were added to the previous solution to carry out the conventional base-catalyzed sol–gel process. The as-prepared solution was maintained for another 12 h at 75°C; this was followed by cooling down to room temperature [Fig. 1(b)].

Synthesis of the SHS coating material

The SHS coating was coated with 200 mL of coating solution (with a weight ratio of MTES-based silsesquioxane spheres solution to FPA solution of about 5) with spin coating at 1500 rpm onto the slide of the CRS substrates and dried under ambient conditions at 110°C for 15 min in the oven [Fig. 1(d)].

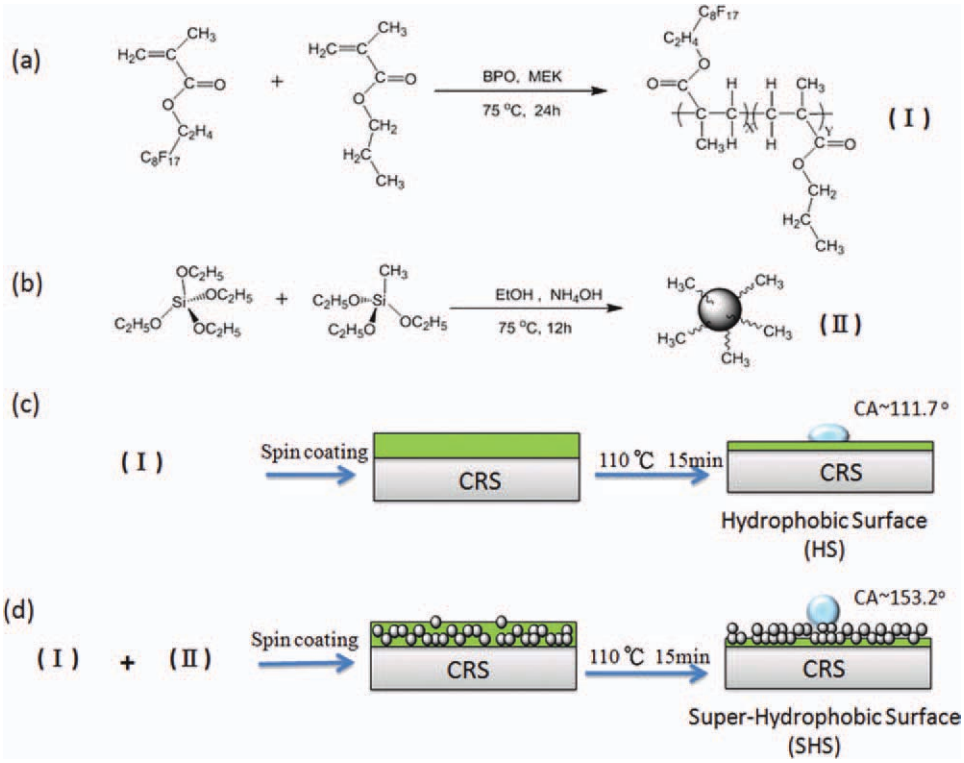

Figure 1 Preparation of the (a) hydrophobic coating solution, (b) MTES–silioca spheres, (c) HS coating, and (d) SHS coating. [Color figure can be viewed in the online issue, which is available at wileyonlinelibrary.com.]

RESULTS AND DISCUSSION

Determination of the sphere size and sphere size distribution

DLS and SEM imaging were used to study the particle size and particle size distribution of the spheres. Although DLS is primarily used as a tool to estimate the particle size range, the results of these experiments could still be used to estimate the particle size and distribution in the colloidal silica sol, as shown in Figure 2(a). The spherical morphology of the product was confirmed by SEM, and the micrograph shown in Figure 2(b) established that the particles did not agglomerate in the solid state. The particle sizes of the MTES-based silsesquioxane spheres, as evaluated by SEM and dynamic light scattering, were about 390 and 405 nm, respectively. The MTES-based silsesquioxane spheres showed a smaller mean particle size through SEM compared to DLS; this was in agreement with observations by van Helden et al.[24] for colloidal silica sols of Stöber silica, Catone and Matijevic[25] for spherical aluminum hydroxide particles, and McDonald et al.[26] for poly(vinyl chloride) latexes. This could be attributed to the shrinkage of the silica structure upon drying and also upon the interaction with the electron beam.[24]

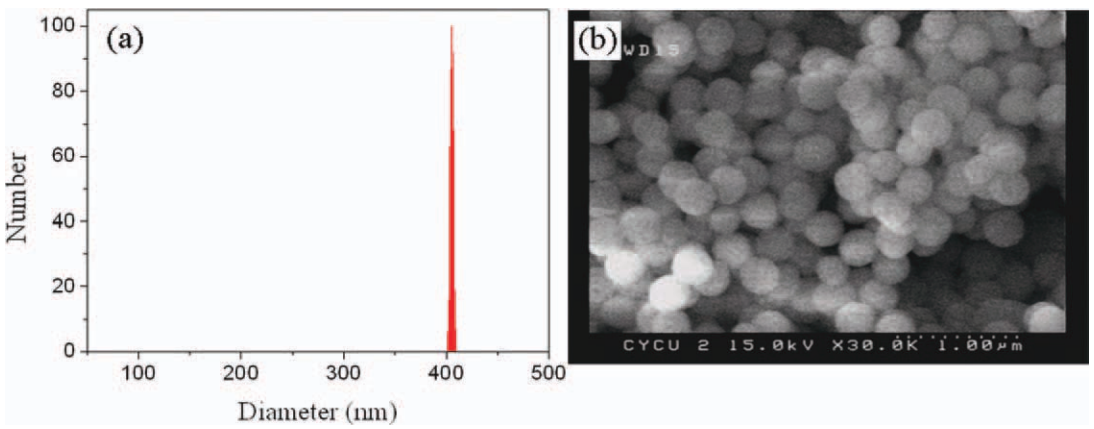

Figure 2 (a) Size distribution of the MTES–silica spheres and (b)SEM images of the MTES-based silsesquioxanes spheres. [Color figure can be viewed in the online issue, which is available at wileyonlinelibrary.com.]

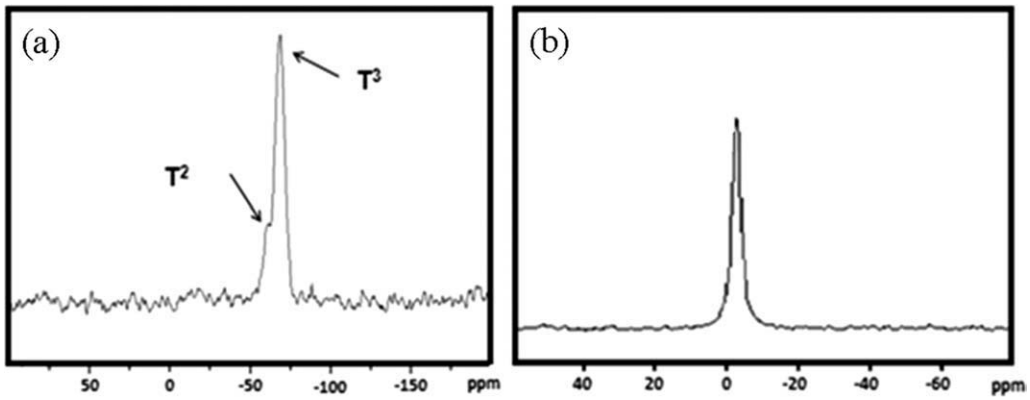

Figure 3 (a) ^{29}Si CP–MAS and (b) ^{13}C MAS NMR spectra.

Chemical spectral studies

Solid-state ^{13}C-NMR and ^{29}Si-NMR spectra are powerful tools for characterizing the chemical structure of powders prepared from organoalkoxysilanes.[27] Solid-state MAS ^{29}Si-NMR spectra provide quantitative information about the condensation reaction, whereas solid-state ^{13}C-NMR spectra are particularly useful for determining the extent of the hydrolysis reaction. The solid-state MAS ^{29}Si-NMR spectra of the silica spheres are shown in Figure 3(a). The peaks at −80.09 and −71.25 ppm in the ^{29}Si-NMR spectra of the MTES-based silsesquioxane spheres could be assigned to fully condensed T^3 and T^2 species, respectively. The T^1 peak was too small to be identified in the spectra. On the other hand, the formation of T^1 and T^0 species was negligible; this suggested that no unreacted organically modified precursor was present.[28] Figure 3(b) shows the solid-state CP/MAS ^{13}C-NMR spectra of the silica spheres, which exhibited an extra resonance peak at chemical shifts of $\delta = -2.8$ ppm. This peak could have been due to the carbon signal from the methyl group of MTES.

The chemical composition of the SHS composite films were investigated with ATR–FTIR spectroscopy. Several characteristic absorption peaks were observed between the range of 700–4000 cm^{-1}. The ATR–FTIR spectra of the MTES–silica spheres and the HS and SHS composite films are shown in Figure 4.

The peak at 1094 cm^{-1} corresponded to Si—O—Si asymmetric stretching vibrations.[29] The presence of this peak confirmed the formation of a network structure inside the film, whereas the absorption bands observed at 800 cm^{-1} were due to the Si—C bonds.[30] On the other hand, the characteristic absorption of the C=C bond at 1640 cm^{-1} disappeared; this indicated that the monomers were polymerized. It should also be noted that unreacted monomers were few and seemed to have evaporated during film formation; hence, their characteristic peaks did not appear in the ATR–FTIR spectra. The characteristic stretching peak of the C=O group was found to be strong at 1730 cm^{-1}. The IR absorption peaks between 1100 and 1240 cm^{-1} could be attributed to the peaks associated with motions of the CF_2 groups at 1203 and 1143 cm^{-1}.[31]

Surface morphological studies

The morphologies of both the HS and SHS coatings were investigated with a water contact meter, SEM, and AFM. The resulting surface morphology of the bare CRS surface and the image of its corresponding water contact angle are shown in Figure 5(a). The surface of the bare CRS substrate was smooth; the water droplet spread onto the substrate because the water contact angle of the bare CRS substrate was about 74.1°. The surface morphology of the CRS substrate applied with the HS coating is presented in Figure 5(b). The water contact angle of the CRS

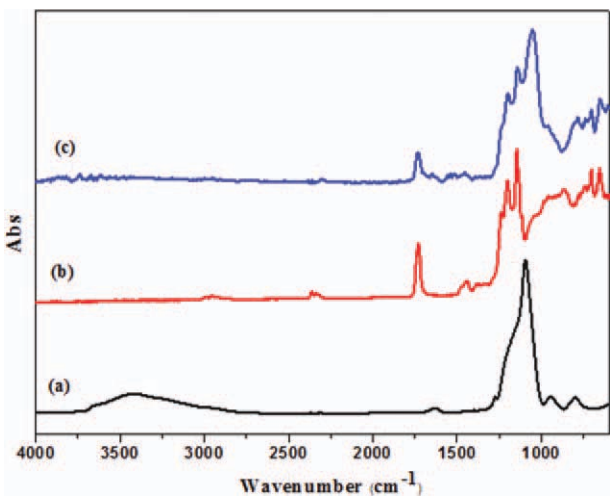

Figure 4 ATR–FTIR spectra of the (a) MTES–silioca spheres, (b) HS, and (c) SHS. [Color figure can be viewed in the online issue, which is available at wileyonlinelibrary.com.]

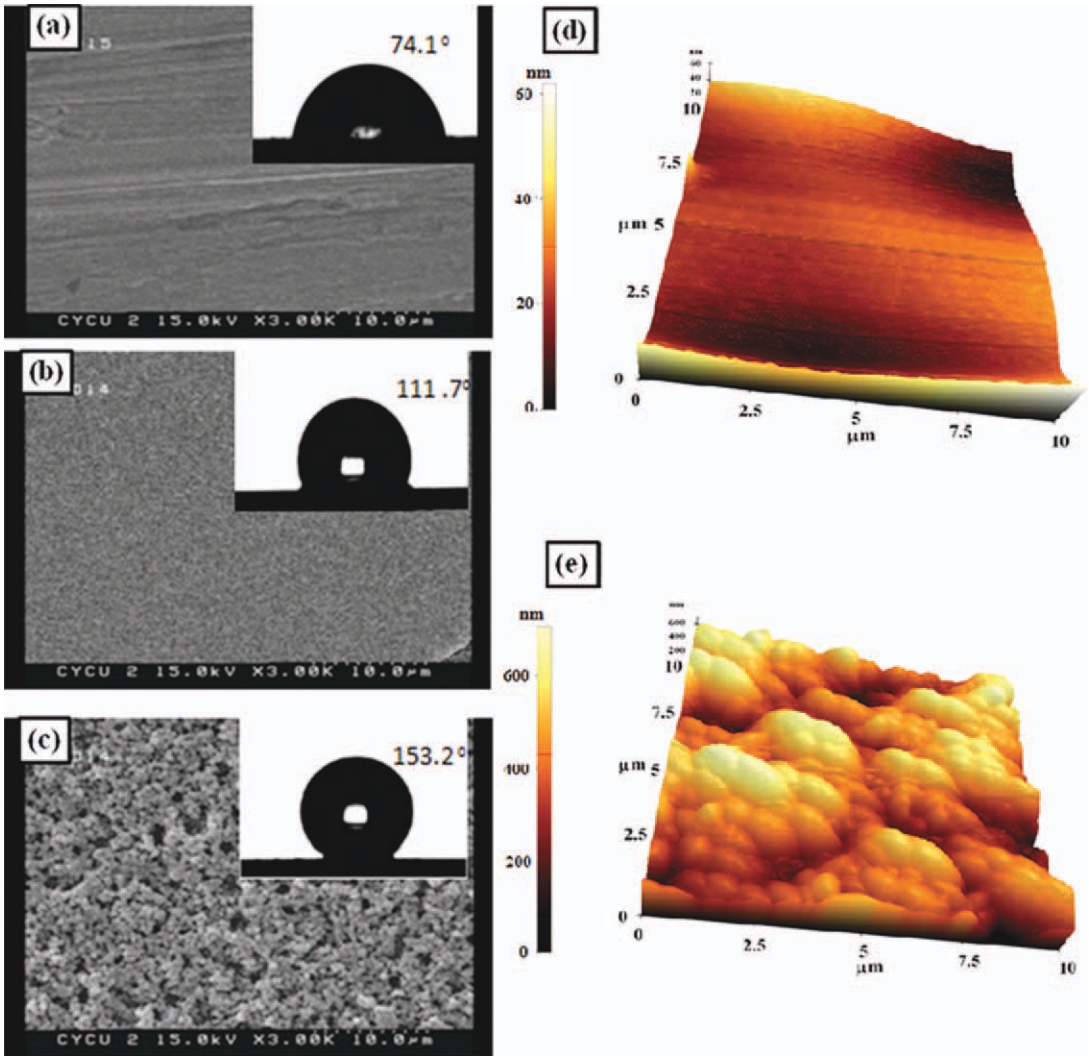

Figure 5 Relationship between R_a and the water contact angle on the CRS substrates: (a) bare CRS, (b) HS on CRS, and (c) SHS on CRS. Optical images of the water contact angles are in the top-right corner of the SEM images. AFM topography images of (d) HS on CRS and (e) SHS on CRS. [Color figure can be viewed in the online issue, which is available at wileyonlinelibrary.com.]

substrate applied with the HS coating was found to be significantly increased from 74° to about 111.7°.

Moreover, Figure 5(c) shows the surface morphology of the substrate applied with the FPA coating and incorporated with MTES-based silsesquioxane spheres; this provided an appropriate surface roughness (R_a) to the substrate. Because the surfaces of the MTES-based silsesquioxane spheres were covered with low-surface-energy FPA materials, the water contact angle was improved from 111.7 to 153.2° accordingly.

The HS was found to be flat, as could be observed in the three-dimensional images obtained by AFM. R_a was also found to be about 6.178 nm [Fig. 5(d)]. However, it was also apparent that the surface became quite rough (R_a was ca. 114.8 nm) and developed a hill-like structure when the CRS was covered with the SHS coating [Fig. 5(e)].

Evidently, the nanostructured composite particles were able to confer a higher water contact angle. As a large amount of air was trapped in the cavities between the nanostructured particles, water could only make contact with the tips of the microsized silica particles. Hence, the water deposited on the SHS was likely resting on an air cushion.

To fully understand the superhydrophobic properties of the surface coating, we described the contact angle in terms of the Cassie equation:[32]

$$\cos\theta_r = f_1 \cos\theta - f_2$$

where θ_r (153.2°) is the contact angle of the SHS, θ (111.7°) is the surface-coated FPA on the side of the bare CRS,[33] and f_1 and f_2 are the fractional interfacial areas of the surface structure of the assembled silica

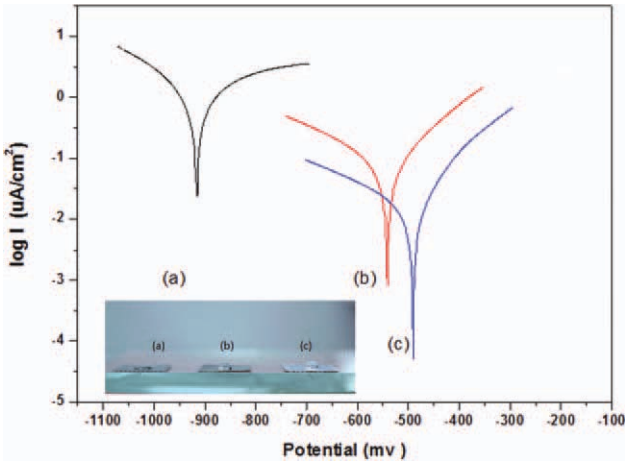

Figure 6 Tafel plots for (a) bare CRS, (b) HS on CRS, and (c) SHS on CRS at 30 ± 0.5°C. Water drop on the (a) CRS, (b) HS, and (c) SHS are in the lower left corner. [Color figure can be viewed in the online issue, which is available at wileyonlinelibrary.com.]

particles bound by FPA and of the air in the interspaces among the surface structure, respectively (i.e., $f_1 + f_2 = 1$). This equation predicts that an increase in the fraction of air (f_2) would increase the contact angle of the surface (θ_r). According to the equation, the f_2 value of the rough surface could be estimated to be around 0.8413. This means that air occupied about 84.13% of the contact area between the water droplet and the rough surface, which was formed by the assembled silica particles that were partly responsible for the superhydrophobic properties of the surface.

The corrosion-preventive ability of a coating depends on three aspects: (1) the water sorption performance of the coating, (2) the transport of water in the coating, and (3) the accessibility to water of the coating/substrate interface. Therefore, it is reasonable to assume that an SHS with low wettability can effectively prevent water from permeating the substrate surface and can exhibit superior corrosion resistance in wet environments.

Potentiodynamic measurements

The corrosion resistance conferred by the HS and SHS coatings was investigated by direct-current polarization, where the lower the I_{corr} was obtained, the better the corrosion resistance was. The samples were immersed in a corrosive medium (3.5 wt % NaCl aqueous electrolyte) for 30 min before testing. The corrosion-preventive effect of the SHS coating was observed to be better than the HS coating and the bare CRS, as shown in Figure 6. Tafel plots for the sample-coated CRS electrode measured at an operational temperature of 30 ± 0.5°C gave an E_{corr} of −490 mV for SHS, a value more positive than both the bare CRS (E_{corr} = −914 mV) and the HS (E_{corr} = −541 mV). Furthermore, I_{corr} of the CRS electrode coated with SHS was about 14.8 μA/cm^2; this corresponded to a corrosion rate (R_{corr}) of about 0.02 mm/year, a value significantly lower than that of the HS-coated material (82.2 μA/cm^2 and 0.96 mm/year) and bare CRS (1096.3 μA/cm^2 and 12.77 mm/year). These results are summarized in Table I.

A large decrease in I_{corr} was observed when the HS coating was applied directly to the CRS substrate [Fig. 6(b)], but an even larger reduction became apparent with SHS coating [Fig. 6(c)]. R_{corr} (mm/year), on the other hand, could be calculated with the following equation:[34]

$$R_{corr}(\text{mm/year}) = \frac{\left[I_{corr}(\text{A/cm}^2) \times M(\text{g})\right]}{D(\text{g/cm}^2) \times V} \times 3270$$

where I is the current (A/cm^2), M is the molecular weight, V is the valence, D is the density (g/cm^3), and 3270 is a constant. The results indicate that SHS exhibited a better corrosion-preventive effect than HS and bare CRS. They also confirmed the superior corrosion-resistant properties of the SHS coating.

The differences in the corrosion behaviors of the samples, as determined by electrochemical measurement, were evaluated by direct visual observation of the CRS surface, as shown in Figure 7. All of the

TABLE I
Contact Angle, Surface Properties, and Electrochemical Corrosion Measurements of the Bare CRS and HS and SHS Films

	Electrochemical corrosion measurements[a]						
Sample code	E_{corr} versus SCE (mV)	R_p (kΩcm^2)[c]	I_{corr} (μA/cm^2)	R_{corr} (mm/year)	Thickness (μm)	Contact angle (°/H_2O)	R_a (nm)[b]
Bare CRS	−914	0.034	1096.3	12.77	—	74.1	—
HS	−541	0.432	82.2	0.96	0.93 ± 0.10	111.7	6.178
SHS	−490	1.940	14.8	0.02	1.02 ± 0.15	153.2	114.809

[a] An SCE was employed as a reference electrode.
[b] R_a was measured by AFM.
[c] R_p (polarization resistance) was measured by VoltaLab 50.

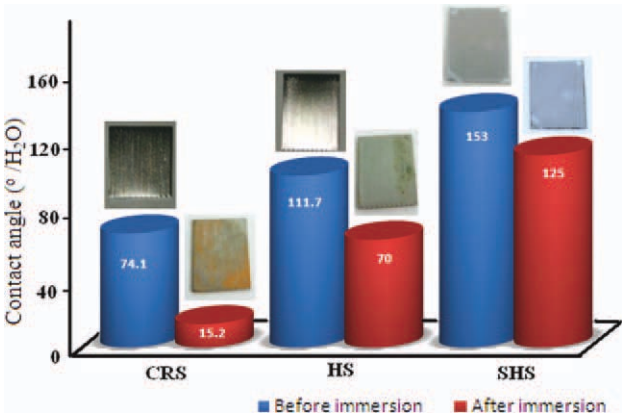

Figure 7 Corrosion durability of the CRS, HS, and SHS surface treatments with immersion in 5 wt % NaCl aqueous electrolyte for 24 h as measured by water contact angle measurement. [Color figure can be viewed in the online issue, which is available at wileyonlinelibrary.com.]

samples were immersed in 3.5 wt % NaCl aqueous electrolyte for 24 h at room temperature. Surprisingly, after immersion for 24 h, the bare CRS was badly corroded. A slight disfiguration also occurred on the surface of the HS coating, and iron rusting appeared on the HS film. However, the surface of the SHS film remained unchanged; this was consistent with the polarization data presented previously. This result confirmed the superior protective ability of the superhydrophobic film.

After this treatment, the contact angle of the bare CRS decreased severely from 74.1 to 15.2° because of iron rusting. The contact angle of the HS decreased from 111.7 to 70°, whereas the SHS only exhibited a small reduction from 153.2 to 125°, as shown in Figure 7. These results indicate that after immersion in the NaCl aqueous electrolyte, the SHS was able to retain its hydrophobic properties and retard corrosion generation. When the SHS was immersed in the NaCl aqueous electrolyte, the air trapped in the SHS surface prevented direct contact between the NaCl aqueous electrolyte and the CRS. Because the SHS coating itself had an intrinsic chemical stability and could not be corroded by the NaCl aqueous electrolyte, the CRS was more ably protected from corrosion by the SHS coating. On the basis of these results, it can be said that SHS provided excellent protection to the CRS substrate against corrosion. The SHS coating was obtained by the embedding of the silica particles into the HS surface. Aside from being responsible for conferring roughness, as evidenced by the hill-like morphology found on the SHS surface, the silica particles could easily trap air in the spaces between these hills.[19] Hence, neither water nor Cl^- (in NaCl aqueous electrolyte) could reach the underlying surface coating (FPA) covering the CRS because of the obstructive effect of these air valleys. Thus, the SHS was able to provide protection and reduce corrosive damage indirectly.

CONCLUSIONS

In this article, we have shown the potential of a novel superhydrophobic coating applied as anticorrosive coating on the basis of a series of electrochemical corrosion protection measurements under saline conditions. This superhydrophobic film provided excellent corrosion protection to the coated CRS substrate and could serve as an effective barrier against aggressive species. The method described in this article could be easily applied in the production of superhydrophobic materials with possible commercial application as a corrosion-preventive coatings for CRS.

Financial support of this research by NSC 98-2113-M-033-001-MY3 is gratefully acknowledged.

References

1. Newman, R. C.; Sieradzki, K. Science 1994, 263, 1708.
2. Chidambaram, D.; Clayton, C. R.; Halada, G. P. J Electrochem Soc 2004, 151, B151.
3. Kuznetsova, A.; Burleigh, T. D.; Zhukov, V.; Blachere, J.; Yates, J. T. Langmuir 1998, 14, 2502.
4. Xin, S.-G.; Song, L.-X.; Zhao, R.-G.; Hu, X.-F. Thin Solid Films 2006, 515, 326.
5. Williams, G.; McMurray, H. N. Electrochem Solid-State Lett 2004, 7, B13.
6. Buchheit, R. G.; Guan, H.; Mahajanam, S.; Wong, F. Prog Org Coat 2003, 47, 174.
7. Yeh, J.-M.; Liou, S.-J.; Lai, C.-Y.; Wu, P.-C.; Tsai, T.-Y. Chem Mater 2001, 13, 1131.
8. Beving, D. E.; McDonnell, A. M. P.; Yang, W. S.; Yan, Y. S. J Electrochem Soc 2006, 153, B325.
9. Choi, J.-K.; Lai, Z.-P.; Ghosh, S.; Beving, D. E.; Yan, Y.-S.; Tsapatsis, M. Ind Eng Chem Res 2007, 46, 7096.
10. Liakos, I. L.; Newman, R. C.; McAlpine, E.; Alexander, M. R. Langmuir 2007, 23, 995.
11. Rapin, C.; D'Huysser, A.; Labbe, J. P.; Gengembre, L.; Steinmetz, P. Rev Métall 1996, 93, 719.
12. Rocca, E.; Steinmetz, J. Corros Sci 2001, 43, 891.
13. Hefter, G. T.; North, N. A.; Tan, S. H. Corrosion 1997, 53, 657.
14. Rammelt, U.; Köhler, S.; Reinhard, G. Electrochim Acta 2008, 53, 6968.
15. Raspini, I. A. Corrosion 1993, 49, 821.
16. Daloz, D.; Rapin, C.; Steinmetz, P.; Michot, G. Corrosion 1998, 54, 444.
17. McCafferty, E.; Wightman, J. P. J Colloid Interface Sci 1997, 194, 344.
18. McCafferty, E. Corros Sci 2003, 45, 1421.
19. Liu, T.; Yin, Y.; Chen, S.; Chang, X.; Cheng, S. Electrochim Acta 2007, 52, 3709.
20. Liu, T.; Chen, S.; Cheng, S.; Tian, J.; Chang, X.; Yin, Y. Electrochim Acta 2007, 52, 8003.
21. Yin, Y.; Liu, T.; Chen, S.; Liu, T.; Cheng, S. Appl Surf Sci 2008, 255, 2978.
22. He, T.; Wang, Y.; Zhang, Y.; Lv, Q.; Xu, T.; Liu, T. Corros Sci 2009, 51, 1757.

23. Chen, S.-G.; Chen, Y.; Lei, Y.-H.; Yin, Y.-S. Electrochem Commun 2009, 11, 1675.
24. van Helden, A. K.; Jansen, J. W.; Vrij, A. J Colloid Interface Sci 1981, 81, 354.
25. Catone, D. L.; Matijevic, E. J Colloid Interface Sci 1974, 48, 291.
26. McDonald, S. A.; Daniels, C. A.; Davidson, J. A. J Colloid Interface Sci 1977, 59, 342.
27. van Blaaderen, A.; Vrij, A. J Colloid Interface Sci 1993, 156, 1.
28. Arkhireeva, A.; Hay, J. N. J Mater Chem 2003, 13, 3122.
29. Hong, J. K.; Kim, H. R.; Park, H. H. Thin Solid Films 1998, 332, 449.
30. Hering, N.; Schriber, K.; Riedel, R.; Lichtenberger, O.; Woltersodorf, J. Appl Organoment Chem 2001, 15, 879.
31. Chen, Y.-J.; Zhang, C.-C.; Chen, X.-X. Eur Polym J 2006, 42, 694.
32. Cassie, A. B. D.; Baxter, S. Trans Faraday Soc 1944, 40, 546.
33. Shi, F.; Wang, Z.; Zhao, N.; Zhang, X. Langmir 2005, 21, 1599.
34. Wei, Y.; Wang, J.; Jia, X.; Yeh, J.-M. Polymer 1995, 36, 4535.